available at www.sciencedirect.com

ScienceDirect

journal homepage: www.elsevier.com/locate/jmbbm

Research paper

Interfacial shear strength in abalone nacre

Albert Yu-Min Lin[a,*], *Marc André Meyers*[a,b,c]

[a] *Materials Science and Engineering Program, University of California, San Diego, La Jolla, CA 92093-0411, USA*
[b] *Department of Mechanical and Aerospace Engineering, University of California, San Diego, La Jolla, CA 92093-0411, USA*
[c] *Department of Nanoengineering, University of California, San Diego, La Jolla, CA 92093-0411, USA*

ARTICLE INFO

Article history:
Received 21 June 2008
Received in revised form
3 February 2009
Accepted 13 April 2009
Published online 3 May 2009

ABSTRACT

The shear strength of the interface between tiles of aragonite in the nacre of red abalone *Haliotis rufescens* was investigated through mechanical tensile and shear tests. Dog-bone shaped samples were used to determine the tensile strength of nacre when loaded parallel to the plane of growth; the mean strength was 65 MPa. Shear tests were conducted on a special fixture with a shear gap of 200 μm, approximately 100 μm narrower than the spacing between mesolayers. The shear strength is found to be 36.9 ± 15.8 MPa with an average maximum shear strain of 0.3. Assuming the majority of failure occurs through tile pull-out and not through tile fracture, the tensile strength can be converted into a shear strength of 50.9 MPa. Three mechanisms of failure at the tile interfaces are discussed: fracture of mineral bridges, toughening due to friction created through nanoasperities, and toughening due to organic glue. An additional mechanism is fracture through individual tiles.

1. Introduction

The abalone shell is composed of two defined layers: an outer prismatic layer (rhombohedral calcite) and an inner nacreous layer (orthorhombic aragonite) as observed by Nakahara et al. (1982). This investigation focuses on the nacreous region only. Aragonitic $CaCO_3$ constitutes the inorganic component of the nacreous ceramic/organic composite (95 wt% ceramic, 5 wt% organic material) (Menig et al., 2000). Stacked pseudo-hexagonal tiles (~0.5 μm thick and ~10 μm wide) are seen arranged in a 'brick-and-mortar' microstructure (Jackson et al., 1988). An organic matrix (20–50 nm thick) interlayer separates tiles which have crystallographic connection through inorganic mineral bridges ~50 nm wide (Song et al., 2002). The mechanical response of nacre is well documented (Currey, 1977; Jackson et al., 1988; Sarikaya et al., 1990; Sarikaya and Aksay, 1992; Menig et al., 2000; Wang et al., 2001) as the material represents one of the most heavily studied biological materials in the emerging field of biomimetics. Its hierarchical structure has been the center of much research (Laraia and Heuer, 1989; Vincent, 1991; Baer et al., 1992; Srinivasan et al., 1991; Heuer et al., 1992; Sarikaya et al., 1990; Barthelat et al., 2006, 2007) and is responsible for a significant increase in toughening from monolithic aragonite.

* *Corresponding author.*
E-mail address: a5lin@ucsd.edu (A.Y.M. Lin).

1751-6161/$ - see front matter © 2009 Elsevier Ltd. All rights reserved.
doi:10.1016/j.jmbbm.2009.04.003

The mechanisms of toughening at the interface between tiles have been the subject of significant debate. Evans et al. (2001) and Wang et al. (2001) identified the rough nature of the surface of each tile, suggesting that friction created by the asperities present at those surfaces was responsible for the resistance to tile sliding. Katti et al. (2001) and Katti and Katti (2006) used finite element modeling to investigate several strengthening and toughening mechanisms including what they described as interlocks between subsequent tiles. Barthelat et al. (2006, 2007), and Tang et al. (2007) in an extensive experimental–analytical–computational investigation modeled the strength of nacre using an elasto-viscoplastic constitutive response of organic material (worm-like chain model). Their experimental techniques are described by Barthelat et al. (2007). Evans et al. (2001) hypothesized that the organic matrix enabled increased toughening by creating a viscoelastic glue at the interface between adjacent tiles. Song et al. (2002), Song and Bai (2003), Gao et al. (2003), Barthelat et al. (2006) and Meyers et al. (2008) investigated the role of mineral bridges in the mechanical response of the tile interfaces. There is a second element to the hierarchy; growth bands that create a lamellar microstructure. Layers of organic material with a thickness of about 20 μm separate the thicker mesolayers of tiled aragonite, approximately 300 μm thick. These layers are described by Menig et al. (2000) Su et al. (2002), and Lin and Meyers (2005) but are not often mentioned in other reports dealing with the mechanical properties of abalone nacre.

2. Experimental procedures

Tensile tests were performed on 11 samples with loading parallel to the tile planes at a strain rate of 3.3×10^{-5} s^{-1}. Nacre coupons were sectioned from five adult sized shells directly after removal from the living specimens along regions in which the shell had minimal curvature. Coupons were first polished so that the two surfaces were parallel and flat. Two methods were applied to obtain the dog-bone shaped specimens. The rectangular coupons were either sandwiched between two steel molds of dog-bone sample silhouette, or laser cut on a laser cam machine. The length of specimens was ~25.4 mm (Fig. 1(a)). The silhouette was sanded down with a small hand file. The laser cuts resulted in localized heating of the sample and loss of mechanical properties; thus, this method was abandoned and no results from samples created through this method are reported. Specimens were kept in sea water before testing to maintain hydration. They were then mounted in the tensile testing device seen in Fig. 1(b).

The shear tests used an assembly similar to that developed by Menig et al. (2000). The steel assembly can be seen in Fig. 2(a); it is composed of two sliding pistons within a cylindrical sleeve. The sample is loaded in the blank cubic space in the center of the device, with the growth planes parallel to the direction of loading (Fig. 2(b)). The principal difference from the setup used by Menig et al. (2000) was the size of the specimens. The shear testing mount dimensions were such that an "s" spacing smaller than 300 μm was created to isolate the region between mesolayers and not

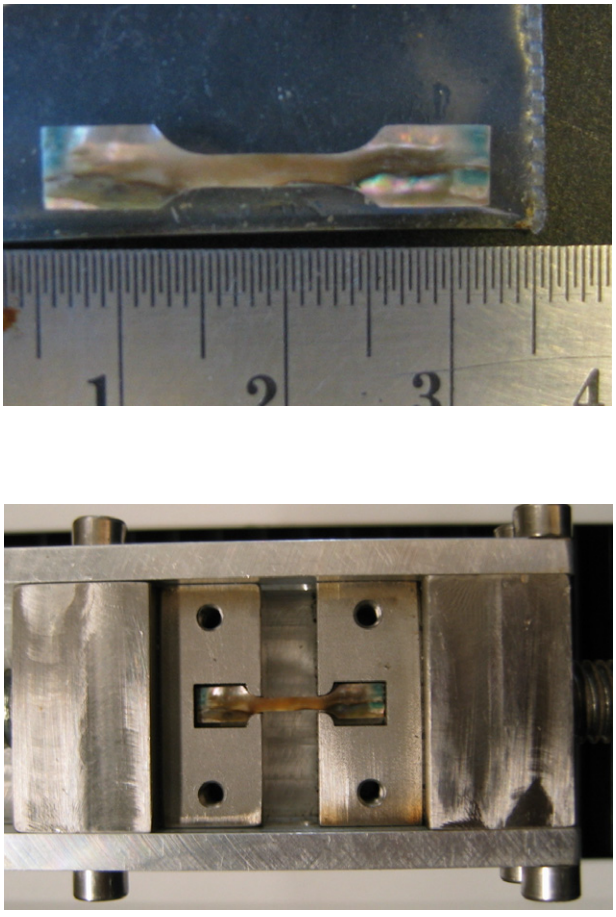

Fig. 1 – Dog-bone mechanical tensile tests on abalone nacre: (a) dog-bone shaped specimen of nacre hydrated in saltwater; (b) dog-bone shaped testing assembly with specimen in place.

across them for testing. Tests were conducted on eight small cubes of nacre with average dimensions $2 \times 2 \times 2$ mm. Cubes were sectioned from adult sized shells directly after removal from a live specimen. Special care was taken to ensure that nacreous sections only were isolated for testing.

3. Results and discussion

Due to the high variability commonly associated with biological materials, a Weibull statistical (Weibull, 1951) analysis was applied to the mechanical testing results. The plot in Fig. 3 shows a 50% failure probability when a stress of approximately 65 MPa was applied. This is within reason to the average tensile strength of the *Gastropods Turbo marmoratus* (116 MPa) and *Trochus niloticus* (85 MPa) reported by Currey (1977). The results are less than a third of the compressive strength reported by Menig et al. (2000) and confirm that the shell sacrifices tensile strength in the perpendicular direction to use it in the direction parallel to the tile structure as stated by Lin et al. (2008).

As mentioned above, shear tests were performed to support previous work by Menig et al. (2000), and to improve

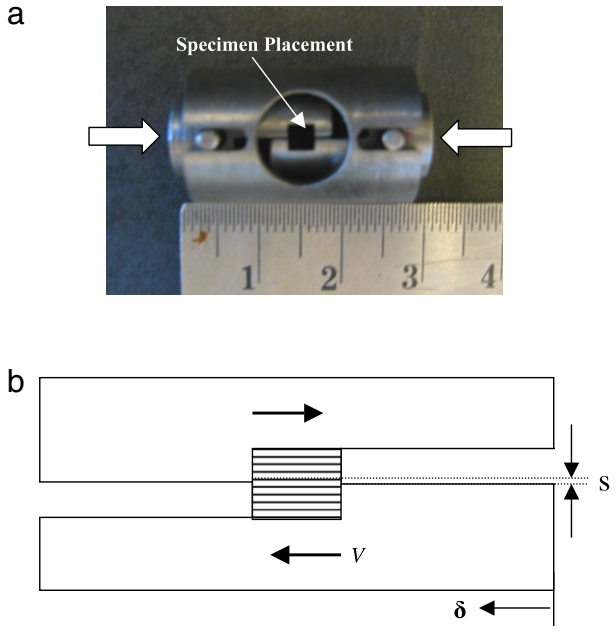

Fig. 2 – (a) Shear testing mount, (b) sketch of shear test configuration acting on a cube of an abalone shell.

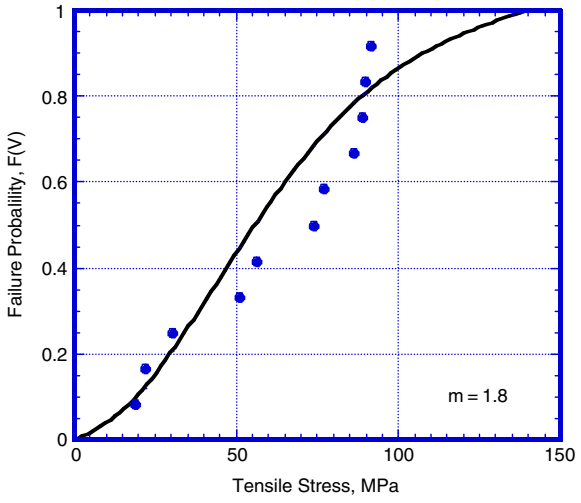

Fig. 3 – The Weibull distribution of tensile strengths with loading parallel to a layered structure. The Weibull modulus "*m*" corresponds to the variability of distributed results; a lower value indicates wider distribution while a wider value indicates a narrower distribution.

upon their effort by scaling down the dimensions of the specimen, isolating the regions of tiled aragonite sandwiched between growth bands. Menig et al. (2000) found empirically that nacre, in shear, exhibited an elastic region up to 12 MPa followed by a linear plastic region up to a maximum shear stress of 30 MPa and maximum shear strain of approximately 0.45. Their setup had a gap "s" (defined in Fig. 2(b)) which was equal to 2 mm; thus the shear action occurred across the macro and microstructure, in contrast with the 200 μm gap

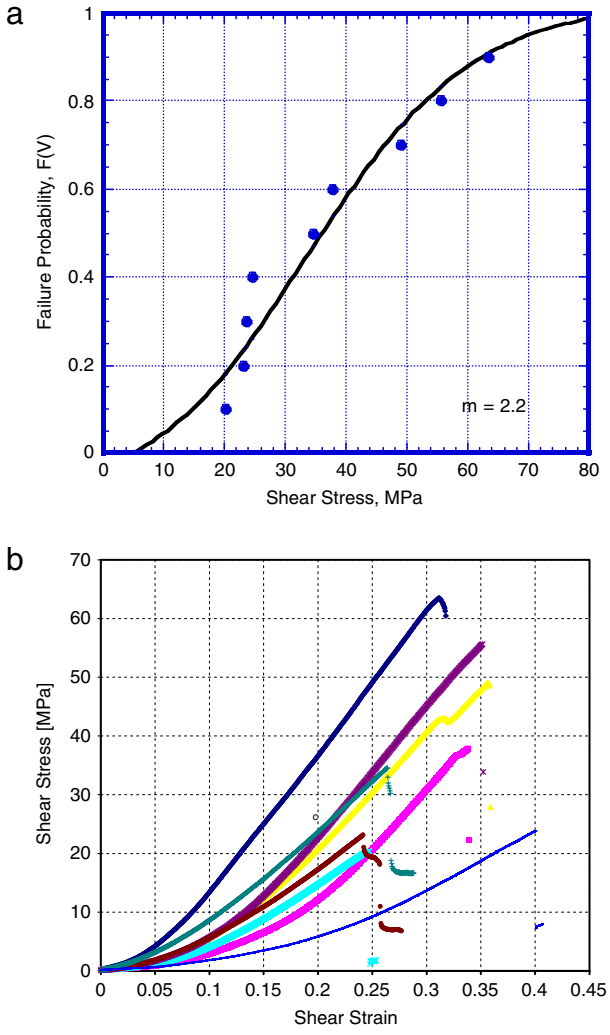

Fig. 4 – Shear tests with loading parallel to a layered structure: (a) The Weibull distribution of shear strengths; (b) stress–strain curves.

"s" in the current study. The shear strain is given by:

$$\gamma = \frac{\delta}{s} \tag{1}$$

in which δ is the axial displacement, and "s" is the gap which defines the region in which shearing action occurs (Fig. 2(b)). The shear stress is simply given by:

$$\tau = \frac{P}{A} \tag{2}$$

where P is the load and A is the area in which shear occurs.

The Weibull distribution of shear strengths is given in Fig. 4(a). The average shear strength was found to be 36.9 ± 15.8 MPa with an average maximum shear strain of approximately 0.3, both remarkably consistent with the results by Menig et al. (2000). However, unlike their tests there is no observed transition from elastic to linearly plastic deformation. As shown in Fig. 4(b) the stress–strain curves indicate an elastic region to a maximum shear strength, followed by catastrophic failure. This may be due to the smaller size of the specimen and the elimination of mesolayers from the process of deformation.

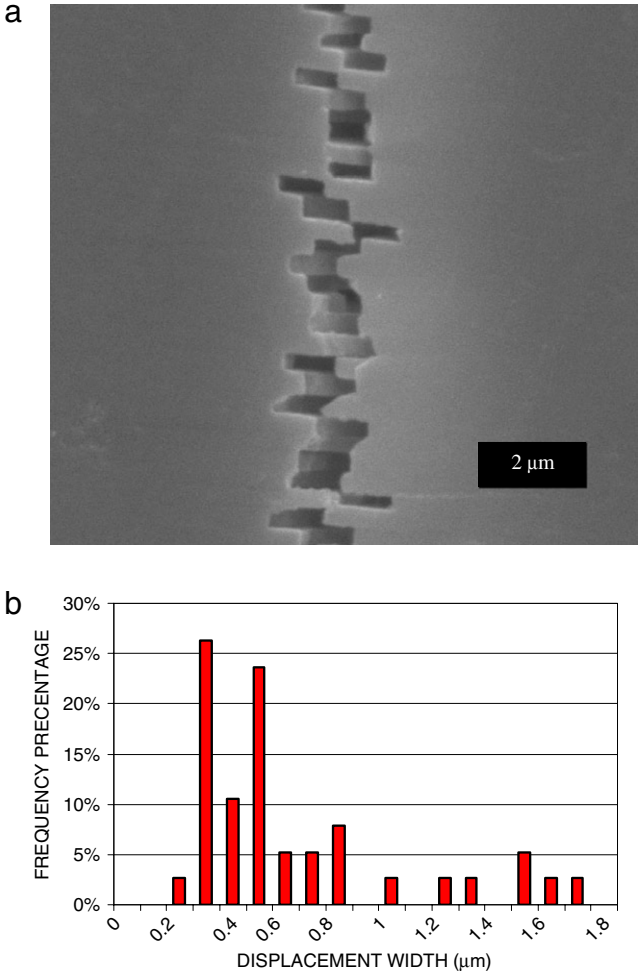

Fig. 5 – (a) SEM micrograph of a polished cross-section after deformation under tension; (b) plot showing the distribution of step lengths.

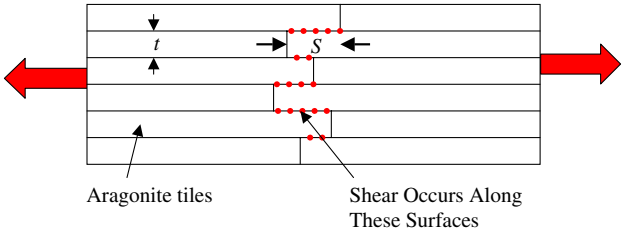

Fig. 6 – Schematic diagram of nacre in tension at the scale of an individual tile.

Fig. 5(a) shows an SEM image of a specimen recovered after being subjected to tension to failure. The dark rectangular features are gaps that opened between tiles during tension. The overlap of tiles was estimated from direct measurements along fracture surfaces, as shown in Fig. 5(b). An average step overlap of 0.63 μm is observed. Nukala and Simunovic (2005) used numerical simulations to show that the tensile strength of nacre was greatly affected by the area of platelet overlap. It can be seen that where tiles separate, the step height corresponds to the overlap. Separation seems

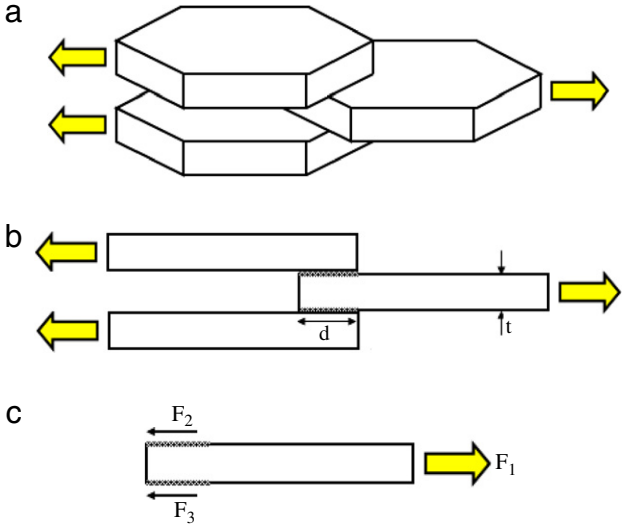

Fig. 7 – Schematic diagram showing pull-out of overlapping tile layers.

to occur through both pull-out and fracture, indicated by irregular fracture surfaces. An optimization of strength ratio between the tensile strength of an individual tile and the shear strength of the interface between overlapping tiles accounts for this observation. Thus, it becomes important to investigate both; we begin with the interface between tiles.

Fig. 6 provides a schematic of nacre in tension at the individual aragonite tile. Fig. 7 shows the schematic representation of tile overlap. Three tiles subjected to tension are shown in Fig. 7(a). A simpler two-dimensional representation is shown in Fig. 7(b). Taking the equilibrium of forces in Fig. 7(c) the relationship between the tensile stress on tile, σ_t, and shear stress on organic interfaces, τ_s, can be calculated:

$$F_1 = F_2 + F_3 \tag{3}$$

$$\sigma_t t = 2\tau_s S. \tag{4}$$

From Fig. 5(b) we can approximate the average step overlap $S = 0.63$ μm and $t = 0.5$ μm:

$$\sigma_t/\tau_s = 2S/t = 2.5. \tag{5}$$

The tensile strength of the ceramic should be at least equal to 2.5 times the shear strength of the interface to ensure shear failure by sliding.

Using Eq. (5), the 50% failure probability tensile stress of 65 MPa (shown in Fig. 1) can be correlated to a shear stress of 26 MPa. An average shear strength of 36.9 MPa is found through shear tests. The discrepancy may be due to the fact that the theoretical shear strength calculated from dog-bone samples assumes that no tiles broke and that shearing occurred through sliding at the interface only.

It is thus possible from the data obtained from dog-bone shaped tensile tests to produce a first hand approximation of the shear stresses experienced by the individual tile interfaces during pull-out. If one assumes that failure in tension occurs by plate pull-out, as seen in Fig. 7(a), then a shear force between tiles can be approximated through the use of Eq. (5).

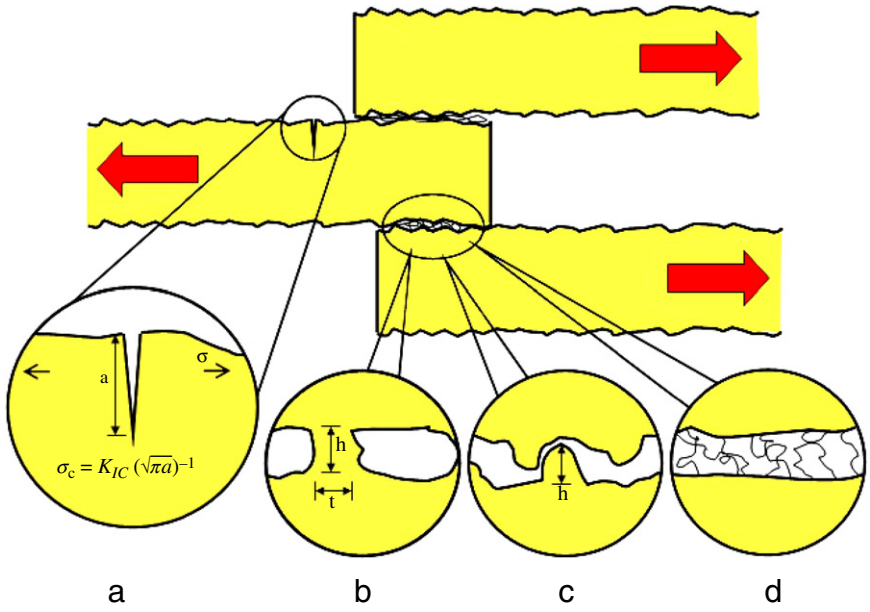

Fig. 8 – Four different failure mechanisms for tension along tile direction: (a) tensile fracture of tile; (b) shear fracture of intertile bridges; (c) shear overcoming friction due to asperities; (d) stretching of organic chains.

The tensile fracture of the tile can be predicted by the simple application of the fracture mechanics equation:

$$\sigma = \frac{K_{Ic}}{\sqrt{\pi a}}. \quad (6)$$

The crack has to travel through tiles for the sliding mechanism to be eliminated. Employing the line of thinking presented by Gao et al. (2003), the strength of each tile is attributed to nanoscale effects originating from flaw confinement due to the dimensions of the tiles. This confinement results in crack configurations of $2a = 0.5$ μm (the thickness of each tile), and $2a = 10$ μm (the length of a tile). Inserting the values of "a" into Eq. (6) while assuming a reasonable value of $K_{IC} = 1$ MPa $m^{1/2}$ results in tensile stresses of $\sigma_t = 1.12$ GPa and 252 MPa. This is not to say that the overall composite would exhibit this near theoretical strength, as clarified by Ballarini et al. (2005), rather the values which are much higher than the shear strength of the tile would encourage failure to occur through the mechanism of tile pull-out, a path of increased toughness.

4. Concluding remarks

Fig. 8 shows the two principal mechanisms of failure when tension is applied parallel to the tile direction: tensile fracture of the tile and sliding along the tile surfaces. The resistance to the sliding of tiles is provided by three possible mechanisms:

(a) Breaking of the nanoscale bridges identified by Song et al. (2002), Lin and Meyers (2005), and Barthelat et al. (2006).
(b) Friction produced by asperities. This was proposed by Wang et al. (2001) as the principal mechanism of toughening at the microscale.
(c) Stretching of organic bonds. This was proposed by Evans et al. (2001) as a valuable mechanism.

The scale of tile dimensions is such that the propagation of internal cracks is limited by the fracture toughness of the material. By constraining the size of internal flaws to the thickness of a tile, a tensile stress $\sigma_t = 1.12$ GPa can be predicted. Seeing as this is not observed in either this report or that of Currey (1977) it is evident that failure occurs more generally though tile pull-out rather than tile fracture. This would account for the increase in toughness observed in nacre over bulk calcium carbonate.

The various mechanisms of failure at the interface provide the intertile shear strength that is partially responsible for the overall mechanical response of the material. Quasi-static shear tests and extrapolated values from dog-bone shaped tensile tests yield shear strengths of 36.9 MPa and 50.9 MPa, for the intertile regions.

Acknowledgements

We would like to thank Ryan Anderson for his assistance at the ITL facility at UCSD and Eddie Kisfaludy for the laboratory facilities at the Scripps Institution of Oceanography. Prof. Joanna McKittrick and Po-Yu Chen are also greatly acknowledged for their insightful contributions. This research is supported by the National Science Foundation Grant DMR 051013.

REFERENCES

Baer, E., Hiltner, A., Morgan, R.J., 1992. Biological and synthetic hierarchical composites. Phys. Today 45, 60–67.
Ballarini, R., Kayacan, R., Ulm, R.J., Belytschko, T., Heuer, A.H., 2005. Biological structures mitigate catastrophic fracture through various strategies. Int. J. Fracture 135, 187–197.

Barthelat, F., Li, C.M., Comi, C., Espinosa, H.D., 2006. Mechanical properties of nacre constituents and their impact on mechanical performance. J. Mater. Res. 21, 1977–1986.

Barthelat, F., Tang, H., Zavattieri, P.D., Li, C.M., Espinosa, H.D., 2007. On the mechanics of mother-of-pearl: A key feature in the material hierarchical structure. J. Mech. Phys. Solids 55, 306–337.

Currey, J.D., 1977. Mechanical properties of mother of pearl in tension. Proc. Roy. Soc. Lond. 196, 443–463.

Evans, A.G., Suo, Z., Wang, R.Z., Aksay, I.A., He, M.Y., Hutchinson, J.W., 2001. Model for the robust mechanical behavior of nacre. J. Mater. Res. 16, 2475–2484.

Gao, H.J., Ji, B.H., Jäger, I.L., Arzt, E., Fratzl, P., 2003. Materials become insensitive to flaws at nanoscale: Lessons from nature. Proc. Natl. Acad. Sci. USA 100, 5597–5600.

Heuer, A.H., Fink, D.J., Laraia, V.J., Arias, J.L., Calvert, P.D., Kendall, K., Messing, G.L., Blackwell, J., Rieke, P.C., Thomson, D.H., Wheeler, A.P., Veis, A., Caplan, A.I., 1992. Innovative materials processing strategies: A biomimetic approach. Science 255, 1098–1105.

Jackson, A.P., Vincent, J.F.V., Turner, R.M., 1988. The mechanical design of nacre. Proc. Roy. Soc. London B 234, 415.

Katti, K.S., Katti, D.R., 2006. Why is nacre so tough and strong? Mater. Sci. Eng. C 26, 1317–1324.

Katti, D.R., Katti, K.S., Sopp, J.M., Sarikaya, M., 2001. 3D finite element modeling of mechanical response in nacre based hybrid nanocomposites. Comput. Theor. Polym. Sci. 11, 397–404.

Laraia, J.V., Heuer, A.H., 1989. Novel composite microstructure and mechanical behavior of mollusk shell. J. Am. Ceram. Soc. 72, 2177–2179.

Lin, A., Meyers, M.A., 2005. Growth and structure in abalone shell. Mater. Sci. Eng. A. 390, 27–41.

Lin, A.Y.M., Chen, P.Y., Meyers, M.A., 2008. The growth of nacre in abalone shell. Acta Biomater. 4, 131–138.

Menig, R., Meyers, M.H., Meyers, M.A., Vecchio, K.S., 2000. Quasi-static and dynamic mechanical response of *Haliotis rufescens* (abalone) shells. Acta Mater. 48, 2383–2398.

Meyers, M.A., Lin, A.Y.M., Chen, P.Y., Muyco, J., 2008. Mechanical strength of abalone nacre: Role of the soft organic layer. J. Mech. Behav. Bio. Mater. 76–85.

Nakahara, H., Bevelander, G., Kakei, M., 1982. Electron microscopic and amino acid studies on the outer and inner shell layers of Haliotis rufescens. Venus Jpn. J. Malac. 41, 33–46.

Nukala, P.K.V.V., Simunovic, S., 2005. A continuous damage random thresholds model for simulating the fracture behavior of nacre. Biomaterials 26, 6087–6098.

Sarikaya, M., Gunnison, K.E., Yasrebi, M., Aksay, J.A., 1990. Mechanical property-microstructural relationships in abalone shell. Mater. Res. Soc. 174, 109–116.

Sarikaya, M., Aksay, J.A., 1992. Nacre of abalone shell; a natural multifunctional nanolaminated ceramic-polymer composite material. In: case, S. (Ed.), Results and Problems in Cell Differentiation in Biopolymers. Springer, Amsterdam, p. 1.

Song, F., Zhang, X.H., Bai, Y.L., 2002. Microstructure and characteristics in the organic matrix layers of nacre. J. Mater. Res. 17, 1567–1570.

Song, F., Bai, Y.L., 2003. Effects of nanostructure on the fracture strength of the interfaces in nacre. J. Mater. Res. 18, 1741–1744.

Srinivasan, A.V., Haritos, G.K., Hedberg, F.L., 1991. Biomimetics: advancing man-made materials through guidance from nature. Appl. Mech. Rev. 44, 463–482.

Su, X.W., Belcher, A.M., Zaremba, C.M., Morse, D.E., Stucky, G.D., Heuer, A.H., 2002. Structural and microstructural characterization of the growth lines and prismatic microarchitecture in red abalone shell and the microstructures of abalone “flat pearls”. Chem. Mater. 14, 3106–3117.

Tang, H., Barthelat, F., Espinosa, H.D., 2007. An elasto-viscoplastic interface model for investigation the constitutive behavior of nacre. J. Mech. Phys. Solids 55, 1410–1438.

Vincent, J.F.V., 1991. Structural Biomaterials. Princeton University Press, New Jersey.

Wang, R.Z., Suo, Z., Evans, A.G., Yao, N., Aksay, I.A., 2001. Deformation mechanism in nacre. J. Mater. Res. 16, 2485–2493.

Weibull, W., 1951. A statistical distribution function of wide applicability. J. Appl. Mech. 18, 293–297.